Theoretical Study of the Interconversion of O_2-Binding Dicopper Complexes

Michaela Flock and Kristine Pierloot*

Chemistry Departement, University of Leuven, Celestijnenlaan 200F, 3001 Heverlee-Leuven, Belgium

Received: February 27, 1998

The structures and interconversion pathway between the $[Cu_2(\mu\text{-}\eta^2\text{:}\eta^2\text{-}O_2)]^{2+}$ and $[Cu_2(\mu\text{-}O)_2]^{2+}$ isomers of model systems with three ammonia ligands per copper center are investigated using both density functional theory with a B3LYP functional (B3LYP-DFT) and multiconfigurational perturbation theory (CASSCF/CASPT2). Both methods lead to thoroughly different results for the relative energy of both isomers. The CASPT2 results reveal an intrinsic stabilization of the $[Cu_2(\mu\text{-}O)_2]^{2+}$ isomer, thus indicating that the presence of a $[Cu_2(\mu\text{-}\eta^2\text{:}\eta^2\text{-}O_2)]^{2+}$ core in the respiratory proteins must be brought back to the presence of bulky capping ligands and/or to external effects caused by solvents and counterions. Both isomers are found to be diamagnetic. For the $[Cu_2(\mu\text{-}\eta^2\text{:}\eta^2\text{-}O_2)]^{2+}$ isomer an antiferromagnetic coupling constant, $-2J$, of 4209 cm^{-1} is calculated at the CASPT2 level. On the other hand, in the $[Cu_2(\mu\text{-}O)_2]^{2+}$ isomer, the lowest ^3B_u state is calculated at 9316 cm^{-1}, but is found to correspond instead to an oxygen $\pi^* \rightarrow \sigma^*$ excitation.

1. Introduction

Due to their ability to transport and activate molecular oxygen, specific dicopper compounds are used as catalysts in chemical and biochemical reactions. Oxygen activation is usually achieved by binding the O_2 molecule between the copper centers. In nature such dicopper systems are found, for instance, in the families of the respiratory proteins hemocyanin (Hc) and tyrosinase. Both are known for O_2 activation, and have been investigated quite thoroughly with various experimental and theoretical methods.[1−12] Both protein types exhibit exceptional spectroscopic features, such as intense absorption bands in the range of 350 and 550 nm, and extremely low (around 750 cm^{-1}) O−O stretching vibrational frequencies, the latter reflecting an increased O−O bond distance in the proteins as compared to free O_2. Among the synthesized and crystallographically characterized model systems *trans*-Cu_2O_2 structures[4,13] with four nitrogen ligands per copper ion are found, but also compounds with a $[Cu_2(\mu\text{-}O)_2]^{2+}$ or a $[Cu_2(\mu\text{-}\eta^2\text{:}\eta^2\text{-}O_2)]^{2+}$ core arrangement, coordinating only three nitrogen ligands per copper ion. The compounds with a $[Cu_2(\mu\text{-}\eta^2\text{:}\eta^2\text{-}O_2)]^{2+}$ core were found to produce electronic spectra which closely resemble the spectra observed for hemocyanin and tyrosinase. A few years ago an X-ray diffraction analysis[9] of oxygenated *Limulus polyphemus*, one member of the hemocyanin family, confirmed the active site to have a $[Cu_2(\mu\text{-}\eta^2\text{:}\eta^2\text{-}O_2)]^{2+}$ core arrangement. EXAFS data[1] revealed that the copper ions in the oxygenated site are in oxidation state II. The same result was also obtained for the above-mentioned model compounds.

Recent experiments[14] on some $[Cu_2O_2]^{2+}$ model complexes have demonstrated that reversible O−O bond cleavage can be achieved by simply exchanging solvents at low temperatures. This is an indication that the interconversion between a $[Cu_2(\mu\text{-}\eta^2\text{:}\eta^2\text{-}O_2)]^{2+}$ and a $[Cu_2(\mu\text{-}O)_2]^{2+}$ core is characterized by a very low energy barrier. When warming up to room-temperature, both species decompose to different bis(μ-hydroxo)dicopper(II) complexes through the cleavage of ligand substituent C−H bonds.

Another intriguing feature of both kinds of copper(II) complexes is their diamagnetic behavior, caused by antiferromagnetic coupling through the oxygen ligands. Experimentally the coupling constant $-2J$ cannot be accurately measured, but a lower limit of 600 cm^{-1} has been determined.[15] So far a theoretical estimate of this constant has only been obtained from broken-symmetry (bs) DFT[8,16] and small valence bond CI[8] calculations.

Models with a $[Cu_2(\mu\text{-}\eta^2\text{:}\eta^2\text{-}O_2)]^{2+}$ core have already been the subject of several theoretical investigations, focusing in particular on the structure[3,5,6,10−12] (also considering different numbers of nitrogen ligands) and on the spectroscopic properties.[5,8] On the other hand, compounds with a $[Cu_2(\mu\text{-}O)_2]^{2+}$ core arrangement have so far received much less attention.[17−19] Recently the interconversion of $[Cu_2(\mu\text{-}\eta^2\text{:}\eta^2\text{-}O_2)]^{2+}$ and $[Cu_2(\mu\text{-}O)_2]^{2+}$ was studied using restricted Hartree−Fock calculations with STO-3G basis sets, followed by single-point complete active space CASSCF/CASPT2 calculations.[16] The results were not really satisfying, probably because of the low accuracy of the RHF structures. Density functional calculations on both cores were also performed previously, using both small[20] and larger nitrogen ligands,[21] and focusing on the influence of the ligand size on the relative stability and isomerization rate between both isomers.

In this work we have studied both $[Cu_2O_2]^{2+}$ cores using DFT and multiconfigurational perturbation theory based on a CASSCF wave function (CASSCF/CASPT2). Simple models with three ammonia ligands coordinated to each copper ion were used. We have analyzed the electronic structure of both cores, and have studied their geometry, relative stability and the barrier of the isomerization path connecting them. Furthermore, calculations on the lowest-lying triplet state(s) have been performed in order to evaluate the extent of antiferromagnetic coupling between the two copper centers in each isomer.

2. Computational Details

Figure 1 depicts the two model systems used in this work, with a $[Cu_2(\mu\text{-}\eta^2\text{:}\eta^2\text{-}O_2)]^{2+}$ core (A), and a $[Cu_2(\mu\text{-}O)_2]^{2+}$ core (B), respectively. Also shown is the orientation of the molecule

* Corresponding author. E-mail: Kristin.Pierloot@chem.kuleuven.ac.be.

10.1021/jp9813241 CCC: $18.00
Published on Web 12/15/1998

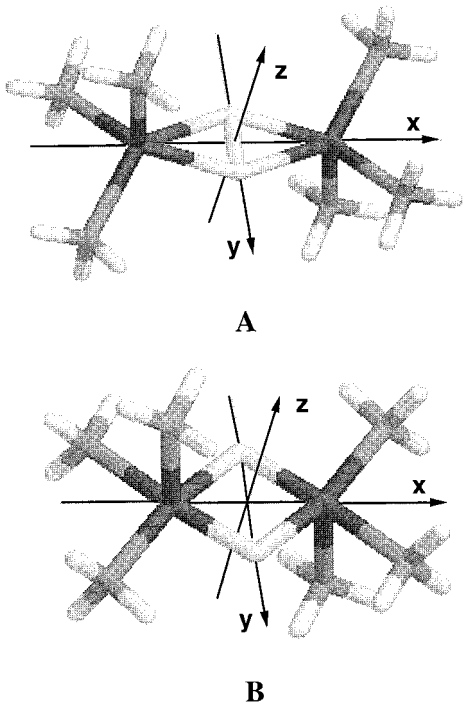

Figure 1. Sketch of structure **A** (above) and structure **B** (below), representing a $[Cu_2(\mu\text{-}\eta^2\text{:}\eta^2\text{-}O_2)]^{2+}$ and $[Cu_2(\mu\text{-}O)_2]^{2+}$ arrangement, respectively. The Cu_2O_2 core of both isomers is located in the *x*,*y*-plane of the coordinate system.

in the coordinate system. The nitrogen ligands are represented by NH_3 groups, thus yielding a very simplified model for the complexes under investigation, which usually contain large tridentate N-donor capping ligands or, in the respiratory proteins, histidine residues.

Geometry optimizations of the singlet and triplet structures were performed at the B3LYP-DFT level using either the *Mulliken-2.25b*[22] or the *Gaussian94*[23] code. Since the implementation of the B3LYP functional is different in both codes, small differences were found for the optimized structures, with deviations of up to 0.004 Å for the bond lengths and up to 0.7 kcal/mol for the relative energies. In all cases a standard fine grid was used together with 6-31G* basis sets for all atoms except copper, for which a double-ζ basis (62111111/3111/311)[24] augmented with diffuse p, d, and f functions was used. The singlet ground state was optimized both using the restricted formalism and the broken-symmetry approach. The latter has already been shown to give an improved description of structure **A**,[4] while leaving structure **B** invariant. This was confirmed by our calculations: the symmetry-broken calculation on structure **B** converged to the restricted solution. All geometry optimizations were performed using C_{2h} symmetry, which is also the symmetry reflected (with small deviations) by the copper ligands in the X-ray structure of oxyhemocyanin[9] and the synthetic models, both with a $[Cu_2(\mu\text{-}O)_2]^{2+}$ and $[Cu_2(\mu\text{-}\eta^2\text{:}\eta^2\text{-}O_2)]^{2+}$ core.[6,18] To check whether the C_{2h} structures really represent minima on the potential energy surface, analytical frequency calculations were performed with *Gaussian94* (on structures optimized with the same code). In case of structure **B**, only positive Hessian matrix eigenvalues were obtained. The calculation on structure **A** revealed two small imaginary frequencies (34 and 42 cm^{-1}), corresponding to rotations within the NH_3 ligands. Both imaginary frequencies still persisted after a reoptimization of the structure without any symmetry restriction. From this we concluded that the C_{2h} structure is indeed a minimum also for structure, and that the two small imaginary frequencies are instead caused by limitations of the fine grid in the *Gaussian94* code. This problem is discussed in detail in refs 25 and 26.

TABLE 1: Core Bond Lengths (Å) of Structures, A, B, and C Obtained from This and Other Work

method	state	Cu−Cu	O−O	Cu−O	Cu−N_{ax}	Cu−N_{eq}
			Structure **A**			
RHF/STO-3G[16]	^1A_g	3.76	1.32			
DFT/BP[21]	^1A_g	3.82	1.44	2.04	2.25	2.09
DFT/B3LYP	^1A_g	3.71	1.40	1.98	2.23	2.06
bs-DFT/B3LYP	^1A_g	3.68	1.45	1.98	2.23	2.06
DFT/B3LYP	^3B_u	3.72	1.50	2.00	2.21	2.06
exp[6]		3.56	1.41	1.92 (av)	2.26	2.00 (av)
oxyHc[9]		3.62	1.36	1.94 (av)	2.33 (av)	1.97 (av)
			Structure **B**			
RHF/STO-3G[18]	^1A_g	2.73	2.28	1.78	2.21	2.00
DFT/BP[21]	^1A_g	2.81	2.37	1.84	2.43	2.03
DFT/B3LYP	^1A_g	2.81	2.29	1.81	2.47	1.99
DFT/B3LYP	^3B_u	2.94	2.29	1.86	2.41	2.03
exp[18]		2.79	2.29	1.83 (av.)	2.31 (av.)	1.99 (av.)
exp[31]		2.78	2.35	1.81 (av.)	2.30	1.99 (av.)
			Structure **C**			
DFT/B3LYP	^1A_g	4.71	1.32	1.95−2.86	2.09	2.07−2.09

The reaction path connecting structures **A** and **B** was studied as follows. First, a series of B3LYP-DFT calculations was performed, keeping the O−O distance fixed in 0.1 Å steps between minima **A** and **B**, while fully optimizing the remaining geometrical parameters. In a second step, single point CASSCF/CASPT2 calculations were performed on the DFT optimized structures along the isomerization pathway. Finally, the Cu−Cu distance of all structures along the reaction path was reoptimized at the CASPT2 level, keeping the other geometrical parameters fixed at their DFT value. No optimizations were performed at the CASSCF level, since it was already shown in a previous study[11,12] on a small $Cu_2O_2^{2+}$ model that CASSCF gives a too large O−O distance, while similar results are obtained for this distance at the DFT and CASPT2 levels.

All CASSCF/CASPT2 calculations were performed with the software package *MOLCAS*-4.0.[27] Medium size atomic natural orbitals (ANO) basis sets[28] (denoted as ANO-S in the MOLCAS basis set library) were used, contracted to [2s] for H, [3s2p1d] for O, [3s2p1d] for N, and [6s4p3d1f] for Cu. The CASPT2 calculations of the structures along the reaction path were based on a CASSCF active space of 8 electrons in 10 orbitals, i.e., both copper $3d_{xy}$ orbitals, the oxygen $2p\sigma$, $2p\sigma^*$ and $2p\pi_x$, $2p\pi_x^*$ orbitals, and four correlating orbitals, namely, copper $4d_{xy}$ and oxygen $3p\sigma$, $3p\pi_x$, $3p\pi_x^*$, one for each active orbital that is doubly occupied in the RHF ground-state configuration. In the CASPT2 calculations all valence electrons, the copper 3d, the oxygen and nitrogen 2s and 2p, and the hydrogen 1s electrons were correlated.

To calculate the singlet−triplet splitting on **A** and **B** a larger active space including also the oxygen (2,3)p(π_z,π_z^*) orbitals was employed, resulting in 12 electrons in 14 active orbitals. This reference wave function was then used for CASPT2 calculations in which only electrons originating from the copper 1s, 2s, and 2p orbitals and the oxygen and nitrogen 1s orbitals were kept frozen. A level shift of 0.3 eV was used in order to remove intruder states.[29,30]

Relativistic effects were accounted for by calculating the mass-velocity and Darwin terms at the CASSCF level and using the CASSCF results to correct the relative energies obtained at the CASPT2 level.

3. Results and Discussion

3.1. Geometrical Features. In Table 1 the geometrical

parameters obtained from a B3LYP-DFT geometry optimization are listed together with previous theoretical results obtained at the RHF/STO-3G level[16,18] and at the DFT level[20,21] using the Becke−Perdew functional. Experimentally determined structural parameters are given for the oxyhemocyanin active site of *L. polyphemus*[9] and for some model compounds.[6,18,31] We believe, however, that a direct comparison of the theoretical results with experiment is not very relevant, considering the limited size of the calculated model system on one hand, and the quite large structural differences found between different structurally characterized $[Cu_2(\mu\text{-}\eta^2\text{:}\eta^2\text{-}O_2)]^{2+}$ and $[Cu_2(\mu\text{-}O)_2]^{2+}$ cores on the other hand. Most important, even for the small model used in this work, a restricted B3LYP-DFT optimization gives rise to two distinct minima, which can clearly be recognized as having a $[Cu_2(\mu\text{-}\eta^2\text{:}\eta^2\text{-}O_2)]^{2+}$ type (structure **A**, with a Cu−Cu distance of 3.71 Å and an O−O distance of 1.40 Å) and a $[Cu_2(\mu\text{-}O)_2]^{2+}$ type (structure **B**, with a Cu−Cu distance of 2.81 Å and an O−O distance of 2.29 Å) core, respectively. At this level **B**, is found to be less stable than **A** by 14.4 kcal/mol. Actually, a third minimum, denoted as **C** in Table 1 was located on the potential surface. This third structure has a trans Cu−O−O−Cu conformation (C_i symmetry), with an O−O distance that is even shorter than in structure **A**, and is found to be 6.5 kcal/mol higher in energy with respect to the latter structure. The structure is reported here for completeness, but will not be further discussed in this work.

An optimization was also performed for the lowest triplet states corresponding to structures **A** and **B**. In both cases, the lowest triplet states are found to have B_u symmetry, and were located at a higher energy than the corresponding ^1A_g state (see also section 3.5): 8.2 kcal/mol in **A**, and 16.0 kcal/mol in **B**. In **A** only the O−O distance increases considerably in ^3B_u as compared to ^1A_g, while in the triplet **B** structure the Cu−Cu distance is elongated by about 0.1 Å.

The importance of performing broken-symmetry (bs) DFT calculations on the $[Cu_2(\mu\text{-}\eta^2\text{:}\eta^2\text{-}O_2)]^{2+}$ core[2] and on dicopper systems in general[32] has already been stressed before. We find that, while the bs-B3LYP calculation on structure **B** converges to the restricted solution, a broken-symmetry optimization of **A** leads to a structure with a slightly shorter Cu−Cu and longer O−O bond, lowering the energy by 5.5 kcal/mol. Recent bs-DFT calculations on the same model system, but using a Becke−Perdew functional,[20,21] converged to the restricted solution for both structures **A** and **B**. It is also noteworthy that both functionals seem to give quite different results for the bond distances (Table 1 in structure **A**, the Cu−Cu distance obtained with Becke−Perdew is more than 0.1 Å longer than the B3LYP result, while in structure **B** the same Cu−Cu distance but a considerably (0.12 Å) longer O−O distance is obtained with Becke−Perdew).

In the (Becke−Perdew) study from Bérces[20,21] the structures obtained for the present model system were also compared to larger models with 1,4,7-triazacyclononane and hydrotris(pyrazolyl)borate modeling the N-donors. Quite large (around 0.1 Å) differences were found for the Cu−Cu, O−O, and also Cu−N_{ax} distances, while the Cu−N_{eq} distances seem to be much less dependent on the specific N-donor. The same is also true for the different experimental structures, showing much less variation in the Cu−N_{eq} than in any other core bond distance. Furthermore, also the theoretical results obtained with different methods for this distance show very little variation, and are all close to the experimental distance. In both structures the axial N ligand is calculated at a much larger distance than the equatorial N ligands, conform with experiment. Moreover, a considerably larger (0.24 Å) Cu−N_{ax} distance is found in **B** than in **A**. This is in accordance with an observation made for the deoxygenated hemocyanins,[33] that smaller axial Cu−N distances are found in structures with longer Cu−Cu distances and vice versa.

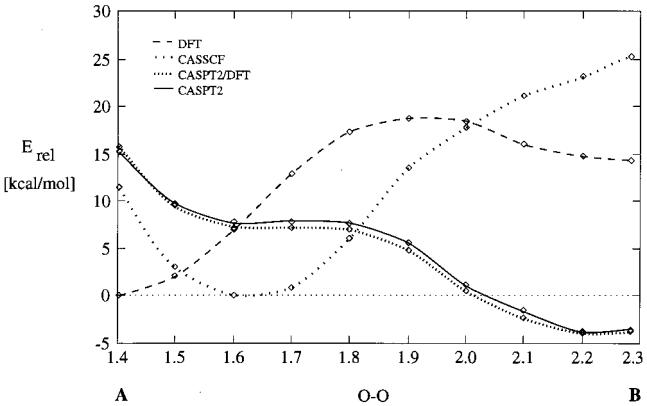

Figure 2. Reaction path on the DFT (dashed line), CASSCF(8in10) (dotted line), and CASPT2(8in10) level on DFT structures (CASPT2/DFT, dotted line with smaller interspacing) and on structures with CASPT2 optimized Cu−Cu distances (full line).

TABLE 2: Relative Energies and Isomerization Barriers (in kcal/mol) for A and B Obtained by DFT and CASSCF/CASPT2 Calculations

method	E_{rel}, **A**	E_{rel}, **B**	$\Delta E_{A\to B}$	$\Delta E_{B\to A}$	structures used
DFT	0.0	14.4	18.7	4.3	DFT/B3LYP
bs-DFT	0.0	19.9	24.2	4.3	bs-DFT/B3LYP
CASSCF(8in10)	0.0	27.1			DFT/B3LYP[a]
CASSCF(8in10)+RC	0.0	23.2			DFT/B3LYP[a]
CASPT2(8in10)	7.3	0.0	0.8	8.1	DFT/B3LYP[a]
CASPT2(8in10)+RC	11.2	0.0			DFT/B3LYP[a]
CASPT2(8in10)	7.8	0.0	0.9	8.7	CASPT2[b]
CASPT2(8in10)+RC	11.5	0.0	0.10	11.6	CASPT2[b]
CASPT2(12in14)	8.8	0.0			CASPT2[b]
CASPT2(12in14)+RC	12.7	0.0			CASPT2[b]

[a] B3LYP structures corresponding to O−O distances of 1.60 Å (**A**) and 2.20 Å (**B**) (the minima of the CASSCF(8in10) and CASPT2(8in10) curves in Figure 3). [b] Only the O−O and Cu−Cu distances are optimized at the CASPT2(8in10) level; see text.

Finally, another indication for the type of bonding of a peroxide between the copper ions is provided by the O−O stretching vibration frequency. In different $[Cu_2(\mu\text{-}\eta^2\text{:}\eta^2\text{-}O_2)]^{2+}$ species this specific vibration was observed at 725−760 cm^{-1},[6,33] while in the $[Cu_2(\mu\text{-}O)_2]^{2+}$ structures values of 590−615 cm^{-1} are measured.[18] The calculated B3LYP result is 612 cm^{-1} for **B**, close to the experimental $[Cu_2(\mu\text{-}O)_2]^{2+}$ value, while for **A** the calculated frequency of the same vibration, 986 cm^{-1}, is significantly higher than experiment. The asymmetric (Cu_2O_2) stretching vibration,[33] observed at 545 cm^{-1} in ref 33 is also computed approximately 200 cm^{-1} lower, i.e., at 340 cm^{-1}.

3.2. Isomerization Pathway. To describe the reaction path for the interconversion reaction between **A** and **B** we chose as the reaction coordinate the O−O distance, which is quite well described for both structures at the restricted B3LYP-DFT level. In a first set of calculations, the O−O distance was kept fixed in 0.1 Å steps between 1.4 and 2.4 Å, while the (restricted) B3LYP-DFT method was used to optimize all other geometrical parameters. The energy profiles obtained from these and further calculations at other computational levels are shown in Figure 2 while the relative energies of structures **A** and **B** the isomerization barriers are collected in Table 2. At the B3LYP-DFT level, the transition state for the interconversion reaction

is found at an O−O distance of 1.9 Å (the corresponding Cu−Cu distance is 3.15 Å). The corresponding energy barrier is 18.7 kcal/mol for the transition **A** → **B** and only 4.3 kcal/mol for the reverse reaction. The $[Cu_2(\mu\text{-}O)_2]^{2+}$ core is found to be less stable than the $[Cu_2(\mu\text{-}\eta^2\text{:}\eta^2\text{-}O_2)]^{2+}$ isomer by 14.4 kcal/mol at this level of theory. Using a Becke−Perdew functional on the same model system[21] a barrierless transition from **A** to **B** was found, the latter structure being less stable by 11.7 kcal/mol. Our bs-DFT calculations only affect the structure and energy of **A**, thus resulting in a further increase of the **B** − **A** energy difference to 19.9 kcal/mol.

In a second step, single point CASSCF(8in10)/CASPT2 calculations were performed on all optimized geometries along the B3LYP-DFT pathway. In the CASSCF calculations, only nondynamical correlation is included. As one can see from Figure 2, the shape of the CASSCF potential curve is thoroughly altered with respect to the corresponding DFT curve. The minimum **A** of is shifted to a larger O−O distance, i.e., 1.6 Å, while the minimum for **B** disappears. Using an O−O distance of 2.2 Å (the minimum found at the CASPT2 level, see below), core **B** is found 27.1 kcal/mol higher in energy than core **A**. The addition of dynamical correlation by means of CASPT2 calculations does not significantly change the position of minimum **A** with respect to the CASSCF results. It is still found at an O−O distance of 1.6 Å (the corresponding DFT value for the Cu−Cu distance is 3.55 Å). Structure **B** is now again found as a minimum at an O−O distance of 2.2 Å (with a corresponding DFT Cu−Cu distance of 2.87 Å). However, the energetics along the reaction path is drastically changed at the CASPT2 level as compared to both CASSCF and DFT. The relative stability of both structures is now reversed, with structure **A** becoming less stable by 7.3 kcal/mol relative to **B**. The reaction barrier for the transition from **A** to **B** is extremely small, 0.8 kcal/mol, while 8.1 kcal/mol is calculated for the reverse reaction. Adding relativistic corrections further lowers structure **B** by 3.9 kcal/mol with respect to **A**. It also flattens the CASPT2 curve, yielding a barrierless transition from **A** to **B**.

To refine the CASPT2 results, we performed at this level an optimization of the Cu−Cu distance at each point (determined by the O−O distance) along the reaction path, while keeping all other parameters fixed as obtained at the restricted B3LYP-DFT level. The overall effect of the CASPT2 treatment on the shape of the reaction curve in Figure 2 is rather small. The location of the O−O minima is not significantly affected. The corresponding Cu−Cu distances are now 3.52 Å (structure **A**, with a O−O distance of 1.60 Å) and 2.94 Å (structure **B**, with a O−O distance of 2.20 Å). These structures are referred to as the "CASPT2" structures in Table 2 and in what follows; note, however, that they do not represent fully optimized structures at this level. The relative energy of structures **A** and **B** is changed to 7.8 kcal/mol without relativistic corrections. When relativistic effects are included the reaction barrier no longer vanishes. The relative energy of the two isomers is found to be 11.5 kcal/mol, with an activation barrier of 0.1 kcal/mol for the **A** → **B** and 11.6 kcal/mol for the **B** → **A** reaction.

The CASPT2 results obtained in this work are thoroughly different from previous results obtained with the same method[16] (but with an active space of 8 electrons in 8 orbitals, smaller basis sets, and using RHF/STO-3G structures), which indicated a very flat potential curve between **A** and **B** without any barrier. They also differ considerably from the results obtained from other studies at the SCF and DFT level. Yet, we believe that the present CASPT2 results should be considered as more reliable, even if, in quantitative terms, they may not represent the final answer, considering the moderate size of the basis sets used in this work and the fact that the CASPT2 structures were not fully optimized. The results show a balanced treatment of structures **A** and **B**. One way to verify this is by checking the weights of the CASSCF reference wave function in the final CASPT2 wave function. These weights give a measure of how large a fraction of the wave function is treated variationally in the CASSCF calculation, and how much is treated by perturbation theory. A prerequisite for the CASPT2 method to give reliable results for relative energies is that the fraction of the wave function treated by CASSCF remains approximately constant. This is the case in the present calculations: with an active space of 8 electrons in 10 orbitals, the CASSCF weights vary only slightly, from 64% to 63%, on going from **A** to **B**. The slightly lower weight obtained for the latter structure is a consequence of the presence of larger dynamical correlation effects, reflected also by its stabilization (leading even to a reversal of the energy order) at the CASPT2 as compared to the CASSCF level. Another way of checking the validity of the CASPT2 results is to go to a larger CASSCF active space. Calculations performed with an active space of 12 electrons in 14 orbitals (see also the methods section) are also included in Table 2. They show a slightly increased weight of the CASSCF reference wave function in the final CASPT2 result, to 68% for structure **A** and 67% for structure **B**, but this does not strongly influence the relative energy of structures **A** and **B**, their final relative energy being 8.8 kcal/mol (without relativistic effects) or 12.7 kcal/mol (with relativistic effects).

The present CASPT2 results indicate that, for the simple models used in this work, structure **B** is more stable than structure **A**. Thus it would seem that $[Cu_2(\mu\text{-}O)_2]^{2+}$ is in fact the intrinsically favored Cu_2O_2 core, and that the stabilization of a core in the proteins and some model systems must be due to effects related to the size and structure of the N-donor ligands and to various external effects caused by the solvent and counterions present. So far, however, any theoretical assessment of these effects has led to conclusions pointing in the opposite direction. A preliminary study of solvent effects,[16] performed using continuum dielectric calculations, indicated that solvation also preferentially stabilizes the $[Cu_2(\mu\text{-}O)_2]^{2+}$ form, and DFT calculations[20,21] (using the Becke−Perdew functional) on dicopper models with larger N-donor ligands, i.e., 1,4,7-triazacyclononane and hydrotris(pyrazolyl)borate, resulted in a relative stabilization of core **B** by 8.8−11.5 kcal/mol as compared to the results obtained with ammonia. On the other hand experimental evidence has been presented recently[19] supporting the validity of the present CASPT2 results. Indeed, from a study of the O_2 reactivity of Cu(I) complexes with various tridentate N-donor ligands it was found that only those ligands in which every carbon in α position to the nitrogen is tertiary may give rise to a $[Cu_2(\mu\text{-}\eta^2\text{:}\eta^2\text{-}O_2)]^{2+}$ structure (given CH_2Cl_2 as a solvent), while any smaller ligand, e.g. with less substituted α carbons, gives a $[Cu_2(\mu\text{-}O)_2]^{2+}$ structure under all conditions. This led to the conclusion that the $[Cu_2(\mu\text{-}O)_2]^{2+}$ core is indeed intrinsically favored, with the $[Cu_2(\mu\text{-}\eta^2\text{:}\eta^2\text{-}O_2)]^{2+}$ form only being observable when sufficient steric bulk is provided by the capping ligands to inhibit isomerization to the smaller O−O bond-broken form.

3.3. Discussion of Nondynamical Correlation Effects. The fact that the results obtained at the B3LYP-DFT and CASPT2 level differ so strongly (a difference of 27 kcal/mol for the relative energies of **A** and **B** is found) is an indication that the B3LYP functional is not capable of providing a balanced

TABLE 3: Percentage Composition of the Valence Active Orbitals in A and B Obtained from the CASSCF(12in14) Calculations

	structure **A**			structure **B**		
orbital	energy	occupation	composition (%)	energy	occupation	composition
$20b_u$	−0.832	1.98	86% O_2 π_x	−0.768	1.92	89% O_2 π_x
$21b_u$	−0.782	1.98	98% O_2 π_z	−0.783	1.98	97% O_2 π_z
$10b_g$	−0.758	1.96	14% Cu d + 83% O_2 π_x^*	−0.815	1.77	41% Cu d + 55% O_2 π_x^*
$22a_g$	−0.750	1.89	100% O_2 σ	−0.743	1.85	92% O_2 σ
$11b_g$	−0.654	1.97	100% O_2 π_z^*	−0.743	1.97	99% O_2 π_z^*
$12a_u$	−0.506	1.20	96% Cu d	−0.634	1.56	58% Cu d + 39% O_2 σ*
$12b_g$	−0.374	0.80	86% Cu d + 11% O_2 π_x^*	−0.296	0.45	59% Cu d + 36% O_2 π_x^*
$13a_u$	0.017	0.11	98% O_2 σ*	−0.301	0.44	38% Cu d + 60% O_2 σ*

treatment of the large correlation effects occurring in both isomers. This failure might be related to the fact that correlation effects, both nondynamical and dynamical, are thoroughly different for both structures. The results from the previous section have already indicated that much more important dynamical correlation effects occur in the $[Cu_2(\mu\text{-}O)_2]^{2+}$ (**B**) than in the $[Cu_2(\mu\text{-}\eta^2\text{:}\eta^2\text{-}O_2)]^{2+}$ (**A**) conformation. In the present section we discuss the nondynamical correlation effects, included in the CASSCF wave function, and show that also this part of the correlation strongly differs between both structures.

This is illustrated in Table 3, where we have collected information concerning the valence orbitals included in the CASSCF(12in14) active space in structures **A** and **B**. The table shows the composition of the natural orbitals (only Cu d and O_2 p are included; other (small) contributions come from Cu s,p and NH_3). Orbital energies are not defined for the natural orbitals, but were taken from the corresponding canonical orbitals, obtained from the diagonalization of the generalized Fock matrix used to build the CASPT2 zeroth-order Hamiltonian. A diagram connecting the orbitals which are the most important for the discussion is presented in Figure 3.

As can be seen from the occupation numbers, the most important correlation effects in structure **A** are concentrated in the HOMO−LUMO orbital pair $12a_u$, $12b_g$, consisting of the positive and negative combinations of the Cu $3d_{xy}$ orbitals, with some contribution of oxygen π_x* in $12b_g$. 89% of the CASSCF wave function (consisting of 537 907 configuration state functions in total) is built from the two closed-shell configurations with either $12a_u$ (53%; this is the HF solution) or $12b_g$ (36%) doubly occupied. When going to structure **B**, however, some drastic changes occur in the composition of the ground-state wave function. Looking first at the energies of the active orbitals, we notice the strong increase (from 0.132 to 0.338 au) in the $12a_u-12b_g$ gap, caused by the approach of the two Cu ions. On the other hand, the simultaneously increasing O−O distance reduces the energy gap between the bonding and antibonding combinations of the oxygen 2p orbitals. This is in particular true for the σ* orbital $13a_u$, which is drastically lowered in energy in **B** as compared to **A** (and in fact becomes the LUMO). Together with these energy changes, the composition of some of the orbitals is also strongly altered, reflecting a much stronger covalent copper−oxygen interaction. The $12a_u$ HOMO now consists of a bonding combination of Cu $3d_{xy}$ and O_2 σ*, with the corresponding antibonding combination found in $13a_u$. On the other hand, the orbitals $10b_g$, $12b_g$ contain the bonding−antibonding combinations of Cu $3d_{xy}$ and O_2 π_x*. The latter four orbitals are also the ones involved in nondynamical effects in structure **B**. As one can see from Table 3, they all have occupation numbers differing strongly from either two or zero. In the CASSCF wave function, the HF configuration is now found with a 59% weight. Many other important configurations appear, involving double excitations from $10b_g$, $12a_u$ into $12b_g$, $13a_u$. However, none of these configurations is found with a weight larger than 7%. This may also explain the different behavior of the broken-symmetry DFT calculations for structures **A** and **B**. The configuration wave function in structure **A** represents a typical two-electrons-in-two-orbitals magnetic coupling problem, for which symmetry-broken calculations may provide an alternative solution. The fact that the bs-DFT calculation on structure **B** converges to the restricted solution reflects the inadequacy of this method to treat the more complicated situation in the latter structure, with only one leading but overall a much larger number of important configurations.

3.4. Formal Charge on Copper in Both Isomers. The present results may also shed some new light on the discussion regarding the formal oxidation states of the copper ions in both structures. Based on EXAFS experiments the copper ions of both structures were proposed to be in oxidation state II.[1] However, Mahapatra et al.[18] suggested that the formal oxidation state of the copper centers in structure **B** is not II but III based on a comparison of the copper−oxygen distances in various Cu(II) and Cu(III) complexes and on a bond valence sum analysis. The present calculations do not provide any direct information concerning formal oxidation states. However, indirect information may be obtained from a comparison of the Cu 3d population resulting from a Mulliken population analysis in both structures. At the B3LYP-DFT level, a lower Cu 3d population is indeed found in structure **B** than in structure **A**: 9.22 e versus 9.55 e, although the former number does certainly not point to a (+3) charge on Cu. On the other hand, the CASSCF(12in14) results give exactly the same Cu 3d population, 9.22 e, for both structures. This result contradicts a previous analysis,[19] based on CASSCF calculations with a smaller (8in8) active space. It was argued there that the strongly increased occupation number of the $13a_u$ orbital in structure **B** as compared to structure **A** (see Figure 3) goes together with a transfer of electrons from Cu 3d to O 2p, thus resulting in a decreased Cu 3d occupation. However, the orbital scheme presented in Figure 3 and the composition shown in Table 3 show that this is only part of the story. First, in structure **B** all four relevant orbitals exhibit a strong delocalization over Cu 3d−O 2p (a point which was also noted in ref 19) such that a redistribution of electrons between them does not produce any considerable transfer of charge between Cu and O. Second, the Cu → O electron transfer in the orbitals $12a_u$, $13a_u$ is counteracted by an opposite transfer in the $10b_g$, $12b_g$ orbitals, thus resulting in a net zero charge transfer, and consequently in a constant Cu 3d occupation in **B** as compared to **A**.

3.5. Antiferromagnetic Coupling. One of the remarkable properties of the Cu_2O_2 systems under consideration is their antiferromagnetic behavior, expressing itself in the lack of EPR signals for both structures. Experimentally only a lower limit of 600 cm^{-1} has been established for the ground-state magnetic

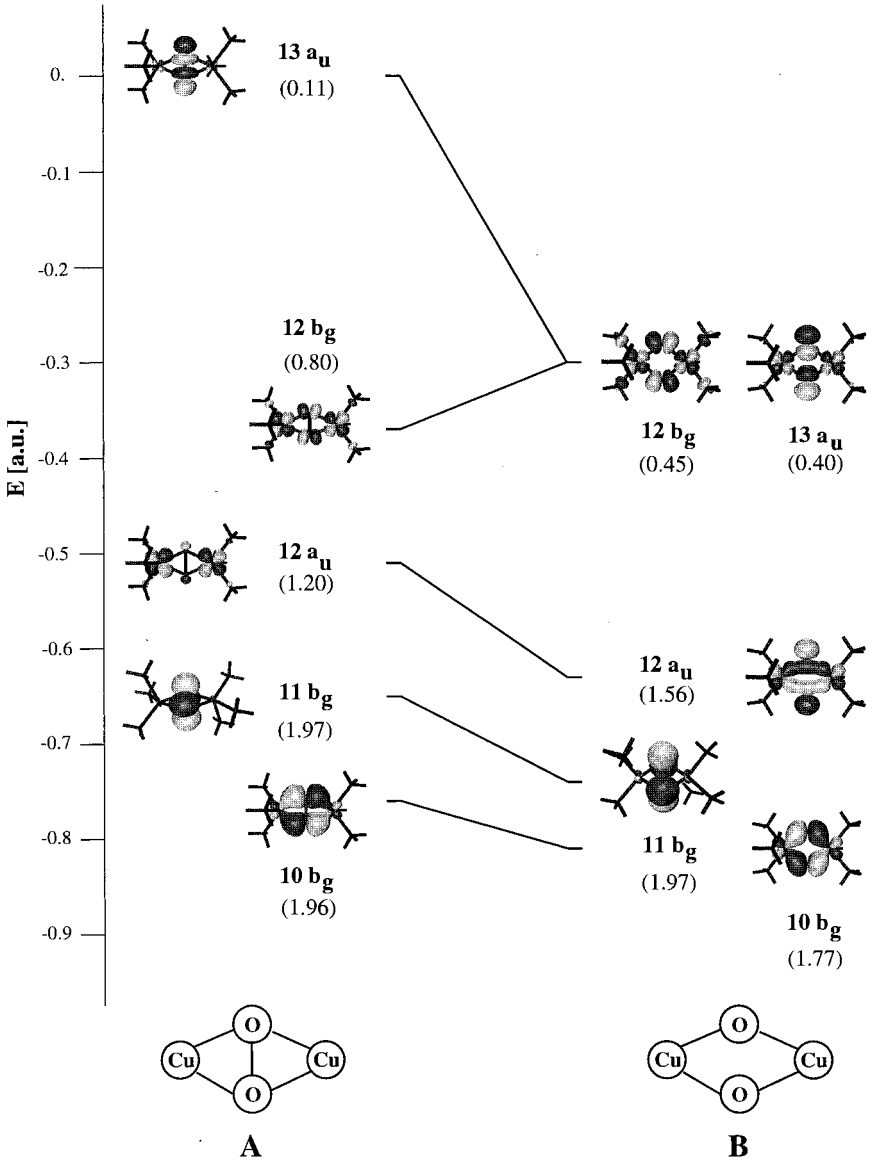

Figure 3. Frontier orbitals and their occupation numbers (in parentheses) for **A** (left) and **B** (right) as obtained by CASSCF(12in14) calculations on the CASPT2 structures.

coupling constant $-2J$ of structure $[Cu_2(\mu\text{-}\eta^2\text{:}\eta^2\text{-}O_2)]^{2+}$.[34,35] Accurate theoretical results are thus needed. One way to evaluate the magnetic coupling constant $-2J$ is by calculating the splitting between the lowest ^1A_g and ^3B_u states. For the $[Cu_2(\mu\text{-}\eta^2\text{:}\eta^2\text{-}O_2)]^{2+}$ models, results obtained from broken-symmetry X_α-SCF scattered wave,[4] valence bond CI,[8] DFT,[20,12] and broken-symmetry DFT[16] calculations are available. Only the latter two studies also report the singlet−triplet splitting for the $[Cu_2(\mu\text{-}O)_2]^{2+}$ structure. Table 4 collects the results obtained from the present and all previous studies.

The previously calculated values for the coupling constant of core **A** cover a range from 2480 to 6163 cm^{-1}. A recent study of Ruiz et al.[32] on several dicopper systems indicated that accurate results for the magnetic coupling constant may be obtained at the DFT level, provided a B3LYP functional in a broken-symmetry approach is used. With this approach, we obtain a $-2J$ value of 5209 cm^{-1} for **A** (using the bs-DFT structure; see Table 1). The results obtained from CASPT2 calculations (on the CASPT2 structure) are not thoroughly different. With an active space of 8 electrons in 10 orbitals, the calculated splitting is 4445 cm^{-1}. Going to the larger CASSCF-(12in14) space slightly decreases this value to 4288 cm^{-1}.

TABLE 4: Singlet−Triplet Splitting ΔE_{t-s} (cm^{-1}) in Structures A and B Obtained from This and Other Work

method	ΔE_{t-s} (**A**)	ΔE_{t-s} (**B**)
VB-CI[8]	2480	
DFT[11]	4665	
DFT[20]	6163	3387
bs-DFT[16]	2880	2250
bs-DFT	5209	6552
CASPT2(8in10)	4445	
CASPT2(12in14)	4288	9 039 (^3B_u)
		11 766 (^3A_g)
		15 327 (^3B_g)
		17 254 (^3A_u)
		17 953 (b^3B_u)
CASPT2(12in14) + RC	4209	9 316 (^3B_u)
		12 051 (^3A_g)
		15 650 (^3B_g)
		17 568 (^3A_u)
		18 375 (b^3B_u)
exp[15,34]	≥600	

Adding relativistic corrections does not significantly alter this result, to 4209 cm^{-1}.

The situation in structure **B** is again more complicated. Both previous studies[16,20] report a $^3B_u-^1A_g$ splitting in **B** which is

lower than the corresponding splitting in structure **A**. These results are at least surprising in view of the strongly increased $12a_u-12b_g$ HOMO−LUMO splitting in structure **B** as compared to **A** (see Table 3 and Figure 3). Using B3LYP-DFT, the value for the lowest $^3B_u-{}^1A_g$ splitting in **B** obtained from this work is 6552 cm^{-1}, 1343 cm^{-1} higher than the corresponding result for **A**. However, an examination of the ^3B_u configuration shows that this state does not correspond to the $12a_u \rightarrow 12b_g$ excitation involved in the ground-state magnetic coupling. Instead it involves the promotion of an electron from orbital $11b_g$ (O_2 π_z*) into orbital $13a_u$ (with predominantly O_2 σ* character). This result may be understood from Figure 3 and the energies in Table 3, showing that $13a_u$, not $12b_g$, is the LUMO in structure **B**, while the energy difference between the $12a_u$ HOMO and $11b_g$ HOMO − 1 orbitals is rather small. This also explains why the CASSCF(8in10) active space does not suffice to calculate the lowest ^3B_u state in structure **B**: it does not include the $11b_g$ orbital. With the larger CASSCF(12in14) active space, the calculated CASPT2 energy for the lowest ^3B_u state is 9039 cm^{-1} without, and 9258 cm^{-1} with relativistic corrections added. This result is considerably higher than the corresponding B3LYP-DFT result. The difference may be explained by the presence of severe nondynamical correlation effects, both for the ^1A_g ground state (see previous section) and the ^3B_u state. At the CASSCF(12in14) level, the lowest ^3B_u state is also found to correspond essentially to a $11b_g \rightarrow 13a_u$ transition. However, the weight of the corresponding $11b_g{}^1 13a_u{}^1$ configuration in the CASSCF wave function is as low as 40%, with many other important (doubly and triply excited) configurations appearing.

Using CASSCF(12in14)/CASPT2, the second triplet state of B_u symmetry was also calculated. There we find the $12a_u \rightarrow 12b_g$ excitation, with a weight of 70% in the CASSCF reference. The calculated CASPT2 result for the $b^3B_u-{}^1A_g$ splitting is 17 953 cm^{-1} (18 375 cm^{-1} with relativistic effects included), about four times as large as the corresponding excitation energy in structure **A**.

Finally, we have investigated the possible presence of alternative low-lying triplet states by performing a CASSCF-(12in14)/CASPT2 calculation on the lowest triplet states of all other symmetries. The resulting excitation energies are also shown in Table 4. All three states, ^3A_g, ^3B_g, and ^3A_u were located between the two ^3B_u states. In all cases, relativistic corrections on the excitation energies turned out to be small.

4. Summary

In this work we have reported the results of a comparative study, using either B3LYP-DFT or CASPT2, of the interconversion between the $[Cu_2(\mu\text{-}\eta^2\text{:}\eta^2\text{-}O_2)]^{2+}$ and $[Cu_2(\mu\text{-}O)_2]^{2+}$ isomers of $(NH_3)_3Cu-O-O-Cu(NH_3)_3^{2+}$, the smallest possible model for O_2 activating proteins such as hemocyanin and tyrosinase. Geometry optimizations performed at the B3LYP-DFT level indeed result in two minima on the potential energy surface with the characteristics of either a $[Cu_2(\mu\text{-}\eta^2\text{:}\eta^2\text{-}O_2)]^{2+}$ (**A**) or $[Cu_2(\mu\text{-}O)_2]^{2+}$ core (**B**). Both structures are in reasonably good agreement with experiment, considering the small size of the model used. However, thoroughly different results were obtained at the B3LYP-DFT and CASPT2 levels for the relative energy of both isomers. The origin of this difference has been brought back to the occurrence of severe and strongly varying correlation effects, both nondynamical and dynamical, along the isomerization pathway. It was shown that the B3LYP-DFT method is not capable of treating in a balanced way the different correlation effects in structures **A** and **B**, and that more accurate results are to be expected from a more rigorous treatment of electron correlation, as offered by the CASSCF/CASPT2 method. Broken-symmetry DFT calculations do seem to be able to capture the most important correlation effects in the $[Cu_2(\mu\text{-}\eta^2\text{:}\eta^2\text{-}O_2)]^{2+}$ structure, leading for example to a reasonably correct description of the antiferromagnetic coupling of the copper ions.

Using CASPT2, the $[Cu_2(\mu\text{-}O)_2]^{2+}$ core is found to be more stable by 12.7 kcal/mol than $[Cu_2(\mu\text{-}\eta^2\text{:}\eta^2\text{-}O_2)]^{2+}$ the core. This suggests that the presence of a $[Cu_2(\mu\text{-}\eta^2\text{:}\eta^2\text{-}O_2)]^{2+}$ core in the proteins and some large model systems is due to a stabilization of this core by steric effects caused by the presence bulky N-donor ligands or by external effects caused by the solvent and counterions present. As such, the inclusion of both these effects cannot be avoided in any theoretical model calculation that aims to provide a more realistic description of the interconversion of both isomers. This fact, together with the fact that the most obvious theoretical method to be used for such large model calculations, i.e., density functional theory, has been shown not to be as trustworthy as thought of in the past for calculations of this type, makes the description of these oxygen containing dicopper systems a challenging problem for theoretical chemistry.

Acknowledgment. This investigation has been supported by grants from the Flemish Science Foundation (FWO), the Concerted Research Action of the Flemish Government, and the European Commission through the TMR program (Grant No. ERBFMRXCT960079).

References and Notes

(1) Co, M. S.; Hodgson, K. O.; Eccles, T. K.; Lontie, R. *J. Am. Chem. Soc.* **1981**, *103*, 984.
(2) Ross, P. K.; Solomon, E. I. *J. Am. Chem. Soc.* **1990**, *112*, 5872.
(3) Maddaluno, J.; Giessner-Prettre, C. *Inorg. Chem.* **1991**, *30*, 3439.
(4) Ross, P. K.; Solomon, E. I. *J. Am. Chem. Soc.* **1991**, *113*, 3246.
(5) Baldwin, M. J.; Ross, P. K.; Pate, J. E.; Tyeklar, Z.; Karlin, K. D.; Solomon, E. I. *J. Am. Chem. Soc.* **1991**, *113*, 8671.
(6) Kitajima, N.; Fujisawa, K.; Fujimoto, C.; Moro-oka, Y.; Hashimoto, S.; Kitagawa, T.; Toriumi, K.; Tatsumi, K.; Nakamura, A. *J. Am. Chem. Soc.* **1992**, *114*, 1277.
(7) Baldwin, M. J.; Root, D. E.; Pate, J. E.; Fujisawa, K.; Kitajima, N.; Solomon, E. I. *J. Am. Chem. Soc.* **1992**, *114*, 10421.
(8) Tuczek, F.; Solomon, E. I. *J. Am. Chem. Soc.* **1994**, *116*, 6916.
(9) Ton-That, H.; Magnus, K. *Inorg. Chem.* **1993**, *51*, 65.
(10) Getlicherman, H.; Giessner-Prettre, C.; Maddaluno, J. *J. Phys. Chem.* **1996**, *100*, 6819.
(11) Bernardi, F.; Bottoni, A.; Casadio, R.; Fariselli, P.; Rigo, A. *Int. J. Quantum Chem.* **1996**, *58*, 109.
(12) Bernardi, F.; Bottoni, A.; Casadio, R.; Fariselli, P.; Rigo, A. *Inorg. Chem.* **1996**, *35*, 5207.
(13) Jacobson, R. R.; Tyeklár, Z.; Farooq, A.; Karlin, K. D.; Liu, S.; Zubieta, J. *J. Am. Chem. Soc.* **1988**, *110*, 3690.
(14) Halfen, J. A.; Mahapatra, S.; Wilkinson, E. C.; Kaderli, S.; Young, V. G., Jr.; Que, L., Jr.; Zuberbühler, A.; Tolman, W. B. *Science* **1996**, *271*, 1397.
(15) Karlin, K. D.; Tyeklár, Z.; Farooq, A.; Jacobson, R. R.; Sinn, E.; Lee, D. W.; Bradshaw, J. E.; Wilson, L. J. *Inorg. Chim. Acta* **1991**, *182*, 1.
(16) Cramer, C. J.; Smith, B. A.; Tolman, W. B. *J. Am. Chem. Soc.* **1996**, *118*, 11283.
(17) Mahapatra, S.; Halfen, J. A.; Wilkinson, E. C.; Pan, G.; Cramer, C. J.; Que, L., Jr.; Tolman, W. B. *J. Am. Chem. Soc.* **1995**, *117*, 8865.
(18) Mahapatra, S.; Halfen, J. A.; Wilkinson, E. C.; Pan, G.; Wang, X.; Young, V. G., Jr.; Cramer, C. J.; Que, L., Jr.; Tolman, W. *J. Am. Chem. Soc.* **1996**, *118*, 11555.
(19) Tolman, W. B. *Acc. Chem. Res.* **1997**, *30*, 227.
(20) Bérces, A. *Int. J. Quantum Chem.* **1997**, *65*, 1077.
(21) Bérces, A. *Inorg. Chem.* **1997**, *36*, 4831.
(22) Rice, J. E.; Horn, H.; Lengsfiels, B. H.; McLean, A. D.; Carter, J. T.; Replogle, E. S.; Barnes, L. A.; Maluendes, S. A.; Lie, G. C.; Gutwski, M.; Rude, W. E.; Sauer, S. P. A.; Lindh, R.; Andersson, K.; Chevalier, T. S.; Widmark, P.-O.; Bouzida, D.; Pacansky, G.; Singh, K.; Gillan, C. J.; Carnevali, P.; Swope, W. C.; Liu, B. *Mulliken*™, Version 2.31h, internal release; IBM Corporation: Almaden, 1995.

(23) Frisch, M. J.; Trucks, G. W.; Schlegel, H. B.; Gill, P. M. W.; Johnson, B. G.; Robb, M. A.; Cheeseman, J. R.; Keith, T.; Petersson, G. A.; Montgomery, J. A.; Raghavachari, K.; Al-Laham, M. A.; Zakrzewski, V. G.; Ortiz, J. V.; Foresman, J. B.; Cioslowski, J.; Stefanov, B. B.; Nanayakkara, A.; Challacombe, M.; Peng, C. Y.; Ayala, P. Y.; Chen, W.; Wong, M. W.; Andres, J. L.; Replogle, E. S.; Gomperts, R.; Martin, R. L.; Fox, D. J.; Binkley, J. S.; Defrees, D. J.; Baker, J.; Stewart, J. P.; Head-Gordon, M.; Gonzalez, C.; Pople, J. A. *Gaussian 94*, Revision D.1. Gaussian, Inc.: Pittsburgh, PA, 1995.

(24) Schäfer, A.; Horn, H.; Ahlrichs, R. *J. Am. Chem. Soc.* **1992**, *97*, 2571.

(25) Johnson, B. G.; Frisch, M. J. *Chem. Phys. Lett.* **1993**, *216*, 133.

(26) Johnson, B. G.; Gill, P. M. W.; Pople, J. A. *Chem. Phys. Lett.* **1994**, *220*, 377.

(27) Andersson, K.; Blomberg, M. R. A.; Fülscher, M. P.; Karlström, G.; Lindh, R.; Malmqvist, P.-Å.; Neogrády, P.; Olsen, J.; Roos, B. O.; Sadlej, A. J.; Schütz, M.; Seijo, L.; Serrano-Andrés, L.; Siegbahn, P. E. M.; Widmark, P.-O. *MOLCAS*, Version 4; Lund University: Sweden, 1997.

(28) Pierloot, K.; Dumez, B.; Widmark, P.-O.; Roos, B. O. *Theor. Chim. Acta* **1995**, *90*, 87.

(29) Roos, B. O.; Andersson, K. *Chem. Phys. Lett.* **1995** *245*, 215.

(30) Roos, B. O.; Andersson, K.; Fülscher, M. P.; Serrano-Andrés, L.; Pierloot, K.; Merchán, M.; Molina, V. *J. Mol. Struct. (THEOCHEM)* **1996**, *388*, 257.

(31) Mahapatra, S.; Halfen, J. A.; Tolman, W. *J. Am. Chem. Soc.* **1996**, *118*, 11575.

(32) Ruiz, E.; Alemany, P.; Alvarez, S.; Cano, J. *J. Am. Chem. Soc.* **1997**, *119*, 1297.

(33) Ling, J.; Nestor, L. P.; Czernuszewicz, R. S.; Spiro, T. G.; Franczkiewicz, R.; Sharma, K. D.; Loehr, T. M.; Sanders-Loehr, J. *J. Am. Chem. Soc.* **1994**, *116*, 7682.

(34) Solomon, E. I.; Dooley, D. M.; Wang, R.-H.; Gray, H. B.; Cerdonio, M.; Mogno, F.; Romani, G. L. *J. Am. Chem. Soc.* **1976**, *98*, 1029.

(35) Dooley, D. M.; Scott, R. A.; Ellinghaus, J.; Solomon, E. I.; Gray, H. B. *Proc. Natl. Acad. Sci. U.S.A.* **1978**, *75*, 3019.